Icephobic properties of anti-wetting coatings for aeronautical applications

Federico Veronesi, Giulio Boveri, Julio Mora, Alessandro Corozzi, Mariarosa Raimondo

PII: S0257-8972(21)00537-5

DOI: https://doi.org/10.1016/j.surfcoat.2021.127363

Reference: SCT 127363

To appear in: *Surface & Coatings Technology*

Received date: 21 April 2021

Revised date: 19 May 2021

Accepted date: 22 May 2021

Please cite this article as: F. Veronesi, G. Boveri, J. Mora, et al., Icephobic properties of anti-wetting coatings for aeronautical applications, *Surface & Coatings Technology* (2021), https://doi.org/10.1016/j.surfcoat.2021.127363

Icephobic properties of anti-wetting coatings for aeronautical applications

Federico Veronesi[1,*], Giulio Boveri[1], Julio Mora[2], Alessandro Corozzi[1], and Mariarosa Raimondo[1]

[1]Institute of Science and Technology for Ceramics CNR-ISTEC, Via Granarolo 64, Faenza (RA), 48018 Italy

[2]Ingeniería de Sistemas para la Defensa de España SA, Beatriz de Bobadilla 3, Madrid, 28040 Spain

E-mail addresses: federico.veronesi@istec.cnr.it (F. Veronesi), giulioboveri01@gmail.com (G. Boveri), modsurf4.pers_externo@inta.es (J. Mora), alessandro.corozzi@istec.cnr.it (A. Corozzi), mariarosa.raimondo@istec.cnr.it (M. Raimondo)

[*]Corresponding author at: Institute of Science and Technology for Ceramics CNR-ISTEC, Via Granarolo 64, Faenza (RA), 48018 Italy. E-mail address: federico.veronesi@istec.cnr.it, telephone: +390546699727

ABSTRACT: Ice accretion on surfaces exposed to supercooled drops is a major issue in several fields, especially for aircraft. The severity and hazardousness of this phenomenon largely depends on the environmental conditions met by the surface. Currently, active ice protection systems are applied to limit the risks related to ice accretion on aircraft, but intense efforts are devoted to the development of passive ice protection systems to overcome their limitations. Anti-wetting materials have been explored as potential icephobic surfaces, with the Slippery, Liquid-Infused Porous Surfaces approach (SLIPS) being one of the most innovative and intriguing possible solutions. However, the literature lacks a proper characterization of the behavior of SLIPS in icing wind tunnel tests that simulate the different icing conditions. In our work, we report the fabrication of ceramic-based coatings as per the SLIPS approach, utilizing two different ceramic porous matrixes and several infused liquids; we also assess the ability of these coatings to reduce ice accretion in icing wind tunnel tests in

both glaze and rime icing regimes, as well as their properties in terms of reduced ice adhesion. Observing the remarkable icephobic behavior displayed by these materials in both types of tests, SLIPS gain significant consideration as candidate passive ice protection systems for aeronautical applications.

KEYWORDS: Anti-wetting coatings; liquid-infused surfaces; SLIPS; icephobicity; ice adhesion; icing wind tunnel

1. Introduction

Ice nucleation and accretion is a crucial issue in several aspects of daily life, e.g., it can cause safety issues when ice is formed on the street pavement, blackouts when it occurs on high-voltage power lines, or loss of aerodynamic properties when ice grows on aircraft [1]. During the icing process, many variables influence ice formation [2]. There are three principal types of ice which can result from freezing phenomena:

- Glaze ice, typically obtained when liquid water content (LWC) is high. Glaze ice crystals have irregular shape and transparent appearance;
- Rime ice, usually formed when LWC is low. Rime ice forms opaque crystalline layers composed of round frozen drops separated by air pockets;
- Mixed ice, which presents intermediate properties between glaze and rime ice [3].

The equation which governs the ice type formed by freezing was found by Makkonen [4]:

$$dM/dt = \alpha_1 \cdot \alpha_2 \cdot \alpha_3 \cdot \omega \cdot v \cdot A$$

dM/dt indicates the icing rate, A is the cross-sectional area which depends on the direction of the particle velocity vectors v, ω is the particles concentration in the cold flux, and α_1, α_2 and α_3 are correction factors with values from 0 to 1: α_1 represents the probability of particle-surface collision and depends on the size of the drops in the cold flux, as small particles follow the air streamlines without collisions with the surface while large particles impact on it and start the icing processes. α_2 represents the efficiency of collection of impacting drops on the surface, also known as sticking efficiency; this correction factor is reduced from unity when drops bounce off the surface. α_3 represents the efficiency of ice accretion, i.e., it is the ratio of the rate of icing to the flux density of the particles that stick to the surface. In the case of α_3=1, there is no liquid layer in contact with the surface and no drops run-off, so the icing process takes place in dry conditions leading to the formation of rime ice. When α_3<1 there is

a liquid layer upon the surfaces and the icing process begins from this layer, but some water particles might run off the surface. This case is known as wet growth, leading to the appearance of the glaze ice.

During flight, aircraft meet different environmental conditions which determine the icing regime. The most common types of clouds are stratiform and cumuliform; the first ones usually display lower LWC and favor the formation of rime ice [5], while the latter ones possess higher LWC and lead to glaze ice. Due to its irregular shape and the high LWC, glaze ice is more difficult to detect and remove than rime ice [6]. In fact, when drops are able to coalesce in liquid form, a continuous ice layer with strong bond to the surface is formed. For this reason, the type of ice formed on the aircraft influences the degree of risk for safety.

To avoid the ice adhesion and accretion on aircraft features, different ice protection systems (IPS) have been adopted [7–10]. They are all active (i.e., they require energy input to operate) and are often expensive and time-consuming, as frequent maintenance operations are needed; moreover, the most common on-ground de-icing method involves the spraying of chemical agents, which are hazardous for the environment [11,12]. For this reason, in the last years the search for alternative IPS has intensified, with special efforts devoted to the development of passive methods to avoid the hindrances of active IPS. In this perspective, anti-wetting surfaces gained a lot of interest as candidate passive IPS [13–18]; several research groups have been working on the development of surfaces and coatings able to decrease ice accretion, therefore called icephobic surfaces. Mishchenko et al. [19] highlighted the relationship between the dynamic repellency to liquids and the attitude to ice nucleation and accretion of different coated surfaces: on surfaces with Contact Angle Hysteresis (CAH) as low as 15°, a full retraction of the supercooled drops is expected before ice nucleation occurs. Khedir et al. [20] found a complete drop rebound at temperatures as low as -10°C on superhydrophobic (SH) Teflon-coated surfaces, suggesting their potential icephobic properties in aeronautical applications. Poulikakos's group [21] studied the impact of supercooled

droplets on SH surfaces, highlighting the role of water viscosity on the penetration between structural features of coatings occurring at subzero temperature. The key parameter is again the contact angle hysteresis: high dynamic repellence allows the decrease of the contact time of the droplets on the materials, avoiding ice nucleation and accretion [22].

Another crucial parameter to hinder ice accumulation on aircraft is the adhesion force between ice and aircraft surfaces, i.e., the lower the adhesion force, the easier the shedding of ice layers on surfaces by aerodynamic drag. A material is commonly defined as icephobic if the ice adhesion strength is lower than 100 kPa [23]. Even ice adhesion strength is correlated with CAH: the higher the drop mobility, thus the lower CAH values, the lower the ice adhesion strength [24–26]. During the last years, several research groups found an effect of anti-wetting surfaces on the decrease of ice adhesion strength, giving credit to these materials as passive IPS [27–30]. More recently, the so called Slippery, Liquid-Infused Porous Surfaces (SLIPS) approach [31] has been increasingly adopted to fabricate durable anti-wetting surfaces; briefly, SLIPS are based on the infusion of a low-surface tension liquid in a porous matrix to achieve enhanced repellence towards several liquids. These materials display prolonged durability in operational conditions that usually lead to the failure of regular SH surfaces, i.e., high pressure due to impinging drops. SLIPS have already demonstrated their potential icephobic properties [32–35], however there is no report on their behavior in terms of ice accretion in Icing Wind Tunnel (IWT) tests in glaze and rime icing conditions [36]. Ma et al. [37] tested SLIPS in IWT, but they focused on the retention of water repellence after erosion by impinging droplets, not on actual ice accretion; moreover, only glaze icing conditions were investigated.

In the present work, we developed anti-wetting coatings as per the SLIPS approach, based on different ceramic oxides to act as nanostructured scaffolds for the infused lubricants. The coated surfaces were characterized in terms of reduced ice accumulation in IWT tests in both glaze and rime regimes, as well as in terms of decrease of ice adhesion force, to assess their

icephobic behavior. Combining the excellent properties displayed in both testing conditions, the proposed anti-wetting coatings could find real application in the aeronautical field, in particular when the aircraft interfaces an environment which leads to the formation of glaze ice.

2. Materials and methods

2.1 Preparation of alumina sol

Alcohol-based alumina sol was prepared as described in a previous paper [38]. Aluminum-tri-sec-butoxide (97%, Sigma-Aldrich) was stirred in isopropyl alcohol (99%, Sigma-Aldrich) for 1h at room temperature. Then, ethyl acetoacetate (95%, Sigma-Aldrich) was added as the chelating agent and the solution was stirred for 3h. Finally, water was added dropwise to the solution to promote hydrolysis of the alkoxide and stirring continued for 24h. Particle size distribution of the sol was evaluated by dynamic light scattering (DLS, Zetasizer Nano S, Malvern Instruments). The sol showed a multimodal particle size distribution (Figure 1, blue line). The peak with the highest scattering intensity was centered at 2.2 nm with smaller amounts of aggregated particles.

2.2 Preparation of silica nanosuspension

The suspension of fluorine-bearing silica nanoparticles (NPs) was prepared as follows: ammonium hydroxide NH_4OH (30%, Sigma-Aldrich) was added to ethanol (99%, Sigma-Aldrich) and stirred to complete dissolution. Tetraethylorthosilicate (TEOS 98%, Sigma-Aldrich) was introduced in the solution, then temperature was increased to 60°C. Once the temperature was reached, 1H,1H,2H,2H-perfluoroctyltriethoxysilane (PFOTS 98%, Sigma Aldrich) was added dropwise to the solution to enhance the hydrophobic behavior of silica nanoparticles. DLS analyses of the nanoparticle suspension showed a monodisperse size distribution with a single peak positioned at 481 nm (Figure 1, red line).

2.3 Fabrication of SLIPS by deposition of hybrid coatings

As substrates for IWT tests we used aluminum alloy 7075 T651 NACA 0012 profiles (Figure 2a) with a surface roughness R_a of about 0.5µm. After cleaning with soapy water and ethanol to remove impurities, the substrates were coated as detailed in the next sections. Dip coating was chosen as deposition technique due to the low cost of equipment, its flexibility and operational simplicity for the processing of materials with different sizes and complex morphologies like NACA profiles.

Alumina-based SLIPS samples were fabricated by dip-coating in the alumina sol with a withdrawal speed of 2mm/s and a soaking time of 5s. After drying at room temperature, they were annealed at 400°C for 60min to obtain a crystalline, flat Al_2O_3 layer, then immersed in boiling water for 30min to form flaky boehmite AlOOH, and thermally treated again (400°C, 10min) to stabilize the inorganic film. Subsequently, a fluoroalkylsilane (FAS) solution in isopropyl alcohol (Dynasylan® SIVO CLEAR EC, Evonik) was dip-coated on the underlying boehmite layer (withdrawal speed 2mm/s, soaking time 120s), followed by annealing at 150°C for 30min.

Finally, the samples were infused in perfluoropolyether (PFPE) lubricant oils (Krytox™ GPL 103 and 105, Chemours). These oils differ in viscosity, namely 82 cSt for Krytox 103 and 522 cSt for Krytox 105 (at 20°C). Infusion was performed by manual brushing, followed by drying overnight in vertical position at room temperature to eliminate excess lubricant. These Al_2O_3-based SLIPS samples were labeled AlK103 and AlK105, respectively.

For the fabrication of silica-based SLIPS, the fluorinated silica NP suspension was deposited via dip coating with withdrawal speed of 2mm/s and soaking time 60s. After drying, the samples were thermally treated at 150°C for 30min to complete solvent evaporation and improve coating adhesion. Subsequently, the substrates were infused with either Krytox lubricants (103 and 105) or silicone oil (viscosity 10 cSt, Sigma-Aldrich); the latter was

selected as a more environmentally sustainable alternative to fluorinated PFPE. These SiO_2-based SLIPS samples were labeled SiK103, SiK105 and SiSO, respectively.

The fabrication of samples for adhesion tests followed the same procedures, using flat 7075 T651 aluminum alloy foils (R_a about 0.5 μm, dimensions 100x25 mm^2, Figure 2b) as substrates. Only half of each surface was coated. The hole at the top of the surfaces is necessary to hold the samples in the ice adhesion instrument.

2.4 Surface characterization

The static water contact angle (WCA) with sessile water drops (volume 10 μL) was measured using an optical system (Drop Shape Analyzer DSA30S, Krüss GmbH). The dynamic wetting behavior was evaluated by measuring the contact angle hysteresis (CAH), which was calculated as the difference between the advancing and the receding contact angle of a sessile drop (volume 20 μL). Contact angle measurements were performed only on flat aluminum samples due to the impossibility to place the NACA profiles in the sample holder of DSA30S. Average values were calculated for five to ten measurements on different points of each surface.

2.5 IWT tests

IWT tests were performed in the facilities of Instituto Nacional de Técnica Aeroespacial (INTA, Madrid, Spain). The test section of the IWT is shown in Figure 3.

The IWT is located in a cold climate chamber to guarantee temperature stability during the tests. The precooled samples were fixed at the center line of the chamber (section 15x15 cm^2). Two icing conditions were simulated, namely glaze and rime icing regimes. Testing conditions are reported in Table I.

Wind speed, *u*, was measured using a PCE-PFM 2 probe with a range from 1 to 80 m/s and an accuracy of 2.5%. Median Volume Diameter (MVD) of sprayed particles was evaluated using

a Malvern Spraytec system, equipped with a 300 mm lens able to measure droplets from 0.1 to 900 μm and determine MVD from 0.5 to 600 μm in sprayed atmospheres, with an accuracy of 1%. LWC was calculated via icing blade method [39]. Five one-minute trials of each sample were performed in each icing condition and ice accretion was evaluated by direct weight measurement (i.e., weighing the samples before and after the test). Five specimens for each coating type were tested and the average weight increase was calculated.

2.6 Ice adhesion tests

For ice adhesion tests, the previously reported [40] double lap shear method was adopted. An Instron 5882 Universal Machine (Barcelona, Spain) with a 5 KN load cell placed inside a climate chamber (refrigerated with liquid nitrogen) was used. The load cell was calibrated in the 5–95% range. The ice layer on the surface of the samples was formed the day before the test employing the following procedure: initially, the sides of the test block (mold) were sealed with transparent adhesive tape to prevent water from leaking; then, the mold was filled with water, making sure that no air bubbles were retained. Finally, the specimen was placed inside ensuring that the level of water on both sides of the specimen was the same, reaching 6 mm below the top edge of the mold (Figure 4). The so-prepared molds were then placed in a freezer at −10°C for at least 16h. One hour before the test, the adhesive tape was removed, and any rest of ice accreted over the sample edges was carefully, but quickly, removed using a blade. The molds were placed again in the freezer for one more hour.

The test block was then fixed to the universal machine, previously cooled to the test temperature. The samples were moved quickly from the freezer to the test rig to minimize temperature change in the system, and after the selected test temperature was reached in the chamber, the samples were left to equilibrate for five more minutes before beginning the test.

The displacement speed (10 mm/min) was set, and the test initialized until the sample was completely out of the mold.

Plots of the measured load (N) as a function of displacement (mm) were obtained during the test, and the observed maximum load peak was considered as the adhesion strength between ice and the surface. Three specimens for each coating were tested to calculate the average and the standard deviation. In these tests, SLIPS samples were tested along with uncoated aluminum substrates, but also with other materials that are commonly applied in aeronautics, namely AA6061-T6 aeronautic aluminum alloy (R_a = 0.2 μm) and polytetrafluoroethylene (PTFE, 3 mm-thick film, R_a = 1.6 μm, purchased from J. Morell S.A., Tarragona, Spain).

3. Results and Discussion

3.1 Surface characterization

The wetting data of the different coating typologies are showed in Table II together with those referring to an uncoated aluminum surface as reference.

The different coatings showed a quite similar anti-wetting behavior, with WCA around 120° and CAH lower than or equal to 10°. The only difference was noticed for silicone-infused samples SiSO, having a WCA of about 112°. The decrease of WCA might be explained considering the surface tension γ of the different oils: silicone oil has a slightly higher γ than Krytox oils (see Table III); according to Young's equation[41], lower WCA is expected. Moreover, AlK103 sample stands out for the lowest value of CAH (3 ± 1°).

Figure 5 shows the morphology of the alumina-based coating. Alumina gel films, after treatment with boiling water, led to the formation of the typical hierarchically organized, flower-like structure. The surface structure presents voids with dimensions of about 50 nm able to host and trap lubricants for SLIPS fabrication. Oil retention is achieved thanks to the

chemical affinity between the grafted fluorinated moieties and the oil, and to capillary pressure exerted by the nanoscale voids [42].

On the other hand, the deposition of fluorinated silica led to the formation of nanoparticle agglomerates distributed on the whole surface, as shown in Figure 6. The porous nature of the coating leads to the accommodation of the lubricant oils inside the nanoscale holes distributed on the whole surface. Compared to alumina coatings (Figure 5), silica ones displayed larger pores (up to 1 μm in some points), which might negatively affect the ability to retain infused liquids by capillarity [43].

3.2 IWT tests

The samples subjected to IWT tests were characterized in terms of weight of attached ice after exposure to supercooled droplets flux. The results in terms of ice weight and percentage of ice weight reduction (taking the weight of accreted ice on the uncoated surface as reference) for glaze icing regime are shown in Figure 7.

In glaze icing conditions, all coated samples showed a remarkable effect in terms of decrease in ice accretion. The best result was achieved by the samples coated with fluorinated silica NPs, which were able to reduce ice accretion by as much as 45%. Probably, the spherical nanoscale morphology of silica-based SLIPS is more capable of resisting the impact of supercooled droplets than the thin boehmite lamellae composing alumina-based SLIPS, which eventually displayed higher amounts of accreted ice. Nevertheless, all samples showed improvement with respect to the reference; the worst performing coating, consisting of alumina-based SLIPS infused in Krytox 105 (AlK105), still delivered a 26% reduction of accreted ice compared to the uncoated surface. It is worth to mention that no clear dependence of ice accretion on lubricant viscosity was observed.

On the other hand, in rime icing regime (Figure 8) the effect of SLIPS coatings on ice accretion became less clear. Only the surfaces coated with silica NPs seemed to lead to a decrease in ice accretion of about 10-18%, however significant differences were observed between replicas as shown by the large standard deviation. Meanwhile, alumina-based SLIPS provided no improvement compared to reference profiles. This result could be explained considering the characteristics of the supercooled droplets in each regime: in glaze conditions, the impacting particles have high LWC (1 g/m^3), therefore SLIPS can effectively let them roll off the surface, limiting their adhesion and the consequent formation and growth of ice. In rime regime, the lower LWC (0.5 g/m^3) and the instantaneous freezing of impinging particles did not allow them to slip on the surface, resulting into adhesion and subsequent ice nucleation and accretion. This hypothesis was confirmed by the images captured during the IWT tests. Figure 9 shows different moments of the test in glaze ice conditions for SiSO sample. From t = 0 to 11s, the supercooled drops presented a good mobility on the surface and did not lead to ice nucleation. Then, glaze ice began to nucleate on the sample, but the poor adhesion coupled led to the formation of a fractured ice layer as shown in Figure 10.

In rime icing conditions, the slippery behavior of the functionalized samples was not observed, with the complete ice layer formation in the first seconds of the test (Figure 11). The formation of an ice layer began just 3s in the test (compared to 11s in glaze conditions), localized on the leading edge of the profile, due to the poor mobility of the supercooled droplets and the velocity of the nucleation of the ice. At the end of the test, the rime ice layer had a typical opaque resemblance as shown in Figure 12. The same trend was observed on all coated samples, with no visible differences between different coating formulations; alumina-based SLIPS even showed a slight increase in weight of accreted ice compared to uncoated profiles.

It is not possible to compare the weight of accreted ice in rime and glaze conditions due to differences in ice density and mechanism of accretion; nevertheless, in summary the IWT

tests showed that the designed anti-wetting coatings cause a diminished ice accretion in glaze icing environment compared to untreated aluminum alloy substrates, due to their ability to repel the supercooled particles with high LWC colliding with the sample.

3.3 Ice adhesion tests

For ice adhesion tests, SLIPS were compared to uncoated aluminum substrates as reference, but also other materials that are commonly applied in aeronautics were considered. Specifically, AA6061-T6 aluminum alloy is frequently used in aircraft parts, while PTFE is a hydrophobic material that has been investigated for its potential icephobicity [44,45]. Measured ice adhesion force values are shown Figure 13.

SLIPS displayed much lower ice adhesion force compared to both uncoated substrates (regular aluminum and AA6061-T6). Moreover, SLIPS samples showed weaker ice adhesion than PTFE-coated surfaces. Among SLIPS, the lowest ice adhesion values were obtained when alumina was used as inorganic layer. Alumina-based SLIPS reduced the ice adhesion force by 95% and 94% compared to uncoated aluminum and AA6061-T6, respectively. When silica was the inorganic layer, adhesion force slightly increased; such differences can be explained considering the surface structure of ceramic matrixes of SLIPS. In non-impact ice accretion methods like the one used for double lap tests, the lubricant acts as a barrier to limit the contact area between ice and solid surface. Alumina-based coatings (Figure 5) have a larger fraction of pores on their surface compared to silica-based ones (Figure 6); these pores host the infused liquid, which is ultimately responsible for the low ice adhesion. As a consequence of the trapped infused material into the pores, for alumina-based SLIPS the effective contact area between the solid ceramic matrix and ice is smaller than for silica-based ones, thus leading to reduced ice adhesion force. However, all SLIPS samples showed adhesion force values well below the conventional 100kPa threshold for icephobic surfaces;

moreover, they all showed significant reduction in ice adhesion force also compared to PTFE-coated surfaces, which are usually considered as an effective passive anti-icing method.

As it was pointed in other papers on the icephobic properties of SLIPS [36,46], the low CAH displayed by SLIPS is related to their reduced ice adhesion properties: due to the presence of a lubricant layer that covers surface features, SLIPS offer few pinning sites for the sticking of both drops and ice layers. Even though the alumina-based SLIPS show different CAH value when infused with Krytox of different viscosity, the adhesion force measured results to be the same independently of the type of Krytox adopted. This evidence suggests that the size and shape of nano-pores of the SLIPS scaffold plays a major role in reducing ice adhesion by diminishing contact area; meanwhile, the infused lubricant prevents ice from penetrating between surface features, thus avoiding mechanical interlocking.

Ice adhesion tests results coupled with the data obtained from glaze condition IWT tests confirmed the promising attitude of SLIPS as icephobic surfaces and their potential future application as passive IPS for aircraft. Further testing of the proposed coating materials will be devoted to the evaluation of their ability to retain their icephobic behavior after several test cycles.

4. Conclusions

In our work, we aimed to assess the icephobic behavior of anti-wetting surfaces fabricated according to the SLIPS approach. First, we synthesized nanosuspensions of ceramic materials like alumina and silica; then, we fabricated hybrid ceramic-organic coatings with different nanostructures to act as porous matrixes for the infusion of low-surface tension liquids, in order to achieve hydrophobic behavior and low adhesion of water drops. The coatings were deposited on different aluminum substrates to perform tests in icing conditions. In icing wind tunnel tests, coated NACA profiles were placed in the test section and underwent ice accretion

experiments in glaze and rime icing conditions. In the former ones, all tested SLIPS coatings displayed remarkably diminished ice accretion compared to the uncoated surface; silica-based coatings in particular gave the highest reduction in ice accretion (up to 45%). Such behavior was attributed to the high LWC of supercooled particles in glaze conditions, which allows SLIPS to repel them effectively. In rime conditions, the lower LWC hindered the effect of SLIPS and little to no improvement in terms of ice accretion was observed compared to the uncoated substrate. On the other hand, ice adhesion tests showed that SLIPS can reduce adhesion force of an order of magnitude compared to aluminum alloys; moreover, they outperformed PTFE as icephobic coatings, especially when alumina was adopted as porous matrix due to its flower-like nanostructure. Such behavior can be attributed to the presence of a lubricant layer on the surface, which leads to a lack of pinning sites and hinders mechanical interlocking between ice and surface features. In summary, SLIPS confirmed their great potential as icephobic surfaces in different conditions, thus drawing interest as materials for application in aircraft and all other sectors where ice accretion must be avoided and delayed.

Acknowledgements

The authors would like to acknowledge the Team Members of Applied Vehicle Technology "Assessment of Anti-Icing and De-Icing Technologies for Air and Sea Vehicles" AVT-299, promoted by the NATO Science & Technology Organization, for the precious inputs and networking opportunity.

Funding sources

This research did not receive any specific grant from funding agencies in the public, commercial, or not-for-profit sectors.

REFERENCES

[1] G. Mingione, Flight in icing conditions, (2010) 188.

[2] O. Parent, A. Ilinca, Anti-icing and de-icing techniques for wind turbines: Critical review, Cold Reg. Sci. Technol. 65 (2011) 88–96. https://doi.org/10.1016/j.coldregions.2010.01.005.

[3] A. Amendola, G. Mingione, On the problem of icing for modern civil aircraft, Air & Space Europe. 3 (2001) 214–217. https://doi.org/https://doi.org/10.1016/S1290-0958(01)90098-X.

[4] L. Makkonen, Models for the growth of rime, glaze, icicles and wet snow on structures, Philos. Trans. R. Soc. A Math. Phys. Eng. Sci. 358 (2000) 2913–2939. https://doi.org/10.1098/rsta.2000.0690.

[5] A. V. Korolev, G.A. Isaac, J.W. Strapp, Aircraft escape strategy from supercooled cloud layers, Collect. Tech. Pap. - 44th AIAA Aerosp. Sci. Meet. 5 (2006) 3256–3267. https://doi.org/10.2514/6.2006-265.

[6] A.G. Kraj, E.L. Bibeau, Phases of icing on wind turbine blades characterized by ice accumulation, Renew. Energy. 35 (2010) 966–972. https://doi.org/https://doi.org/10.1016/j.renene.2009.09.013.

[7] J.L. Laforte, M.A. Allaire, J. Laflamme, State-of-the-art on power line de-icing, Atmos. Res. 46 (1998) 143–158. https://doi.org/10.1016/S0169-8095(97)00057-4.

[8] M. Farzaneh, C. Volat, A. Leblond, Anti-icing and de-icing techniques for overhead lines, in: Atmospheric Icing of Power Networks, 2008: pp. 229–268. https://doi.org/10.1007/978-1-4020-8531-4_6.

[9] R.I. Egbert, R.L. Schrag, W.D. Bernhart, G.W. Zumwalt, T.J. Kendrew, An investigation of power une de-icing by electro-impulse methods, IEEE Trans. Power Delivery. 4 (1989) 1855–1861. https://doi.org/10.1109/61.32682.

[10] R.W. Gent, N.P. Dart, J.T. Cansdale, Aircraft icing, Philos. Trans. R. Soc. A Math. Phys. Eng. Sci. 358 (2000) 2873–2911. https://doi.org/10.1098/rsta.2000.0689.

[11] S.R. Corsi, S.W. Geis, J.E. Loyo-Rosales, C.P. Rice, R.J. Sheesley, G.G. Failey, D.A. Cancilla, Characterization of aircraft deicer and anti-icer components and toxicity in airport snowbanks and snowmelt runoff, Environ. Sci. Technol. 40 (2006) 3195–3202. https://doi.org/10.1021/es052028m.

[12] A.I. Freeman, B.W.J. Surridge, M. Matthews, M. Stewart, P.M. Haygarth, Understanding and managing de-icer contamination of airport surface waters: A

synthesis and future perspectives, Environ. Technol. Innov. 3 (2015) 46–62. https://doi.org/10.1016/j.eti.2015.01.001.

[13] M. Susoff, K. Siegmann, C. Pfaffenroth, M. Hirayama, Evaluation of icephobic coatings - Screening of different coatings and influence of roughness, Appl. Surf. Sci. 282 (2013) 870–879. https://doi.org/10.1016/j.apsusc.2013.06.073.

[14] P. Guo, Y. Zheng, M. Wen, C. Song, Y. Lin, L. Jiang, Icephobic/Anti-Icing Properties of Micro/Nanostructured Surfaces, Adv. Mater. 24 (2012) 2642–2648. https://doi.org/10.1002/adma.201104412.

[15] A.J. Meuler, J.D. Smith, K.K. Varanasi, J.M. Mabry, G.H. McKinley, R.E. Cohen, Relationships between water wettability and ice adhesion, ACS Appl. Mater. Interfaces. 2 (2010) 3100–3110. https://doi.org/10.1021/am1006035.

[16] R.D. Narhe, D.A. Beysens, Growth dynamics of water drops on a square-pattern rough hydrophobic surface, Langmuir. 23 (2007) 6486–6489. https://doi.org/10.1021/la062021y.

[17] K.K. Varanasi, T. Deng, J.D. Smith, M. Hsu, N. Bhate, Frost formation and ice adhesion on superhydrophobic surfaces, Appl. Phys. Lett. 97 (2010) 234102. https://doi.org/10.1063/1.3524513.

[18] C. Lee, Y. Nam, H. Lastakowski, J.I. Hur, S. Shin, A.L. Biance, C. Pirat, C.J. Kim, C. Ybert, Two types of Cassie-to-Wenzel wetting transitions on superhydrophobic surfaces during drop impact, Soft Matter. 11 (2015) 4592–4599. https://doi.org/10.1039/c5sm00825e.

[19] L. Mishchenko, B. Hatton, V. Bahadur, J.A. Taylor, T. Krupenkin, J. Aizenberg, Design of ice-free nanostructured surfaces based on repulsion of impacting water droplets, ACS Nano. 4 (2010) 7699–7707. https://doi.org/10.1021/nn102557p.

[20] K.R. Khedir, G.K. Kannarpady, H. Ishihara, J. Woo, M.P. Asar, C. Ryerson, A.S. Biris, Temperature-dependent bouncing of super-cooled water on teflon-coated superhydrophobic tungsten nanorods, Appl. Surf. Sci. 279 (2013) 76–84. https://doi.org/10.1016/j.apsusc.2013.04.038.

[21] T.M. Schutzius, S. Jung, T. Maitra, P. Eberle, C. Antonini, C. Stamatopoulos, D. Poulikakos, Physics of icing and rational design of surfaces with extraordinary icephobicity, Langmuir. 31 (2015) 4807–4821. https://doi.org/10.1021/la502586a.

[22] G. Boveri, A. Corozzi, F. Veronesi, M. Raimondo, Different Approaches to Low-Wettable Materials for Freezing Environments: Design, Performance and Durability, Coatings. 11 (2021) 77. https://doi.org/https://doi.org/10.3390/coatings11010077.

[23] K. Golovin, S.P.R. Kobaku, D.H. Lee, E.T. DiLoreto, J.M. Mabry, A. Tuteja, Designing durable icephobic surfaces, Sci. Adv. 2 (2016) e1501496. https://doi.org/10.1126/sciadv.1501496.

[24] M. Wen, L. Wang, M. Zhang, L. Jiang, Y. Zheng, Antifogging and icing-delay properties of composite micro- and nanostructured surfaces, ACS Appl. Mater. Interfaces. 6 (2014) 3963–3968. https://doi.org/10.1021/am405232e.

[25] L.B. Boinovich, A.M. Emelyanenko, Anti-icing potential of superhydrophobic coatings, Mendeleev Commun. 23 (2013) 3–10. https://doi.org/10.1016/j.mencom.2013.01.002.

[26] S.A. Kulinich, M. Farzaneh, Ice adhesion on super-hydrophobic surfaces, Appl. Surf. Sci. 255 (2009) 8153–8157. https://doi.org/10.1016/j.apsusc.2009.05.033.

[27] Q. Fu, X. Wu, D. Kumar, J.W.C. Ho, P.D. Kanhere, N. Srikanth, E. Liu, P. Wilson, Z. Chen, Development of sol-gel icephobic coatings: Effect of surface roughness and surface energy, ACS Appl. Mater. Interfaces. 6 (2014) 20685–20692. https://doi.org/10.1021/am504348x.

[28] C. Wei, B. Jin, Q. Zhang, X. Zhan, F. Chen, Anti-icing performance of super-wetting surfaces from icing-resistance to ice-phobic aspects: Robust hydrophobic or slippery surfaces, J. Alloys Compd. 765 (2018) 721–730. https://doi.org/10.1016/j.jallcom.2018.06.041.

[29] G. Momen, R. Jafari, M. Farzaneh, Ice repellency behaviour of superhydrophobic surfaces: Effects of atmospheric icing conditions and surface roughness, Appl. Surf. Sci. 349 (2015) 211–218. https://doi.org/10.1016/j.apsusc.2015.04.180.

[30] J. Chen, K. Li, S. Wu, J. Liu, K. Liu, Q. Fan, Durable Anti-Icing Coatings Based on Self-Sustainable Lubricating Layer, ACS Omega. 2 (2017) 2047–2054. https://doi.org/10.1021/acsomega.7b00359.

[31] T.S. Wong, S.H. Kang, S.K.Y. Tang, E.J. Smythe, B.D. Hatton, A. Grinthal, J. Aizenberg, Bioinspired self-repairing slippery surfaces with pressure-stable omniphobicity, Nature. 477 (2011) 443–447. https://doi.org/10.1038/nature10447.

[32] S.B. Subramanyam, K. Rykaczewski, K.K. Varanasi, Ice adhesion on lubricant-impregnated textured surfaces, Langmuir. 29 (2013) 13414–13418. https://doi.org/10.1021/la402456c.

[33] Y.H. Yeong, C. Wang, K.J. Wynne, M.C. Gupta, C.L. Brown, Oil-Infused Superhydrophobic Silicone Material for Low Ice Adhesion with Long-Term Infusion Stability, ACS Appl. Mater. Interfaces. 8 (2016) 32050–32059. https://doi.org/10.1021/acsami.6b11184.

[34] P. Irajizad, M. Hasnain, N. Farokhnia, S.M. Sajadi, H. Ghasemi, Magnetic slippery extreme icephobic surfaces, Nat. Commun. 7 (2016) 1–7. https://doi.org/10.1038/ncomms13395.

[35] F.L. Heale, I.P. Parkin, C.J. Carmalt, Slippery Liquid Infused Porous TiO2/SnO2 Nanocomposite Thin Films via Aerosol Assisted Chemical Vapor Deposition with Anti-Icing and Fog Retardant Properties, ACS Appl. Mater. Interfaces. 11 (2019) 41804–41812. https://doi.org/10.1021/acsami.9b14160.

[36] P. Juuti, J. Haapanen, C. Stenroos, H. Niemelä-Anttonen, J. Harra, H. Koivuluoto, H. Teisala, J. Lahti, M. Tuominen, J. Kuusipalo, P. Vuoristo, J.M. Mäkelä, Achieving a slippery, liquid-infused porous surface with anti-icing properties by direct deposition of flame synthesized aerosol nanoparticles on a thermally fragile substrate, Appl. Phys. Lett. 110 (2017) 161603. https://doi.org/10.1063/1.4981595.

[37] L. Ma, Z. Zhang, L. Gao, Y. Liu, H. Hu, An experimental study on the durability of icephobic slippery liquid-infused porous surfaces (SLIPS) pertinent to aircraft anti-/de-icing, 2018 Atmos. Sp. Environ. Conf. (2018) 1–14. https://doi.org/10.2514/6.2018-3654.

[38] M. Raimondo, M. Blosi, A. Caldarelli, S. Guarini, F. Veronesi, Wetting behavior and remarkable durability of amphiphobic aluminum alloys surfaces in a wide range of environmental conditions, Chem. Eng. J. 258 (2014) 101–109. https://doi.org/10.1016/j.cej.2014.07.076.

[39] S. Goswami, S. Klaus, J. Benziger, Wetting and absorption of water drops on nafion films, Langmuir. 24 (2008) 8627–8633. https://doi.org/10.1021/la800799a.

[40] J. Mora, P. García, R. Muelas, A. Agüero, Hard Quasicrystalline Coatings Deposited by HVOF Thermal Spray to Reduce Ice Accretion in Aero-Structures Components, Coatings. 10 (2020) 290. https://doi.org/10.3390/coatings10030290.

[41] T. Young, An Essay on the Cohesion of Fluids, Philos. Trans. R. Soc. London. 95 (1805) 65–87. https://doi.org/10.1098/rstl.1805.0005.

[42] X. He, P. Cao, F. Tian, X. Bai, C. Yuan, Infused configurations induced by structures influence stability and antifouling performance of biomimetic lubricant-infused surfaces, Surf. Coatings Technol. 358 (2019) 159–166. https://doi.org/10.1016/j.surfcoat.2018.11.035.

[43] P. Baumli, M. D'Acunzi, K.I. Hegner, A. Naga, W.S.Y. Wong, H.-J. Butt, D. Vollmer, The challenge of lubricant-replenishment on lubricant-impregnated surfaces, Adv. Colloid Interface Sci. 287 (2020) 102329. https://doi.org/10.1016/j.cis.2020.102329.

[44] R. Jafari, G. Momen, M. Farzaneh, Durability enhancement of icephobic fluoropolymer film, J. Coatings Technol. Res. 13 (2016) 405–412. https://doi.org/10.1007/s11998-015-9759-z.

[45] J. Gonzales, D. Kurihara, T. Maeda, M. Yamazaki, T. Saruhashi, S. Kimura, H. Sakaue, Novel Superhydrophobic Surface with Solar-Absorptive Material for Improved De-Icing Performance, Materials. 12 (2019) 2758. https://doi.org/10.3390/ma12172758.

[46] H. Niemelä-Anttonen, H. Koivuluoto, M. Tuominen, H. Teisala, P. Juuti, J. Haapanen, J. Harra, C. Stenroos, J. Lahti, J. Kuusipalo, J.M. Mäkelä, P. Vuoristo, Icephobicity of Slippery Liquid Infused Porous Surfaces under Multiple Freeze–Thaw and Ice Accretion–Detachment Cycles, Adv. Mater. Interfaces. 5 (2018) 1–8. https://doi.org/10.1002/admi.201800828.

Table I. Summary of the icing conditions (temperature T, median volume diameter MVD, liquid water content LWC and wind speed u) applied in the icing wind tunnel tests in glaze and rime icing regimes.

Regime	**T (°C)**	**MVD (µm)**	**LWC (g/m^3)**	**u (m/s)**
Glaze	-5	20	1	50
Rime	-15	20	0.5	50

Table II. Average static contact angle with water (WCA) and contact angle hysteresis (CAH) of the different coated surfaces. Standard deviations are reported as errors. Data of the uncoated reference sample are also provided.

Sample	**WCA (°)**	**CAH (°)**
Reference	89 ± 2	59 ± 7
AlK103	122 ± 1	3 ± 1
AlK105	119 ± 2	9 ± 1
SiSO	112 ± 2	10 ± 2
SiK103	123 ± 4	6 ± 2
SiK105	119 ± 5	9 ± 1

Table III. Surface tension (γ) and viscosity (η) of the four lubricants used for SLIPS fabrication. Surface tension was measured with a DSA30S optical system (Krüss GmbH) with the pendant drop method; average values and standard deviations (reported as errors) were calculated for five measurements.

Lubricant Oil	**γ (mN/m)**	**η (cSt)**
Krytox™103 (K103)	17.41 ± 0.01	82[1]
Krytox™105 (K105)	18.35 ± 0.08	522[1]
Silicone Oil 10cSt (SO)	20.01 ± 0.30	9-11[2]
[1]Chemours Technical Specifications of Krytox™ GPL series oils [2]Sigma-Aldrich Product Specification Sheet.		

Figure 1. Distribution of particle size in the alumina sol (Al_2O_3, blue line) and in the fluorinated silica nanoparticle suspension (SiO_2-F), as determined by DLS.

Figure 2. a) 7075 T651 aluminum alloy NACA 0012 profiles adopted as substrates for IWT tests; b) flat aluminum foils adopted as substrates for ice adhesion tests.

Figure 3. Test section of the icing wind tunnel (IWT) at INTA, Spain.

Figure 4. (Left) Test block employed to form ice on both sides of the sample; (right) block attached to the Universal machine ready to start a test.

Figure 5. Scanning electron micrograph of the nanostructured alumina layer.

Figure 6. Scanning electron micrograph of the nanostructured silica layer.

Figure 7. IWT tests in glaze icing regime: (left) weight of accreted ice for uncoated reference and SLIPS samples; standard deviations are reported as error bars. (Right) Average ice weight and percentage of ice weight reduction values for uncoated reference and SLIPS samples. Standard deviations are reported as errors.

Figure 8. IWT tests in rime icing regime: (left) weight of accreted ice for uncoated reference and SLIPS samples; standard deviations are reported as error bars. (Right) Average ice weight and percentage of ice weight reduction values for uncoated reference and SLIPS samples. Standard deviations are reported as errors.

Figure 9. Snapshots of the IWT test of a SiSO sample in glaze conditions: at the beginning of the test (t=0s, left) and after 11s (middle) and 60s (right).

Figure 10. Detail of the ice layer accreted on a SiSO sample after IWT tests in glaze conditions.

Figure 11. Snapshots of the IWT test of a SiSO sample in glaze conditions: at the beginning of the test (t=0s, left) and after 3s (middle) and 60s (right).

Figure 12. Detail of the ice layer accreted on a SiSO sample after IWT tests in rime conditions.

Figure 13. Ice adhesion tests: (left) ice adhesion force for all tested samples; standard deviations are reported as error bars. (Right) Average ice adhesion force values for uncoated reference, AA6061-T6 alloy, PTFE, and SLIPS samples. Standard deviations are reported as errors.

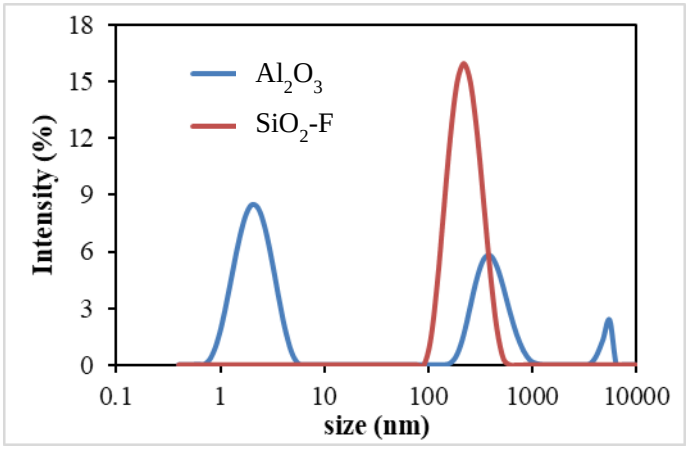

1

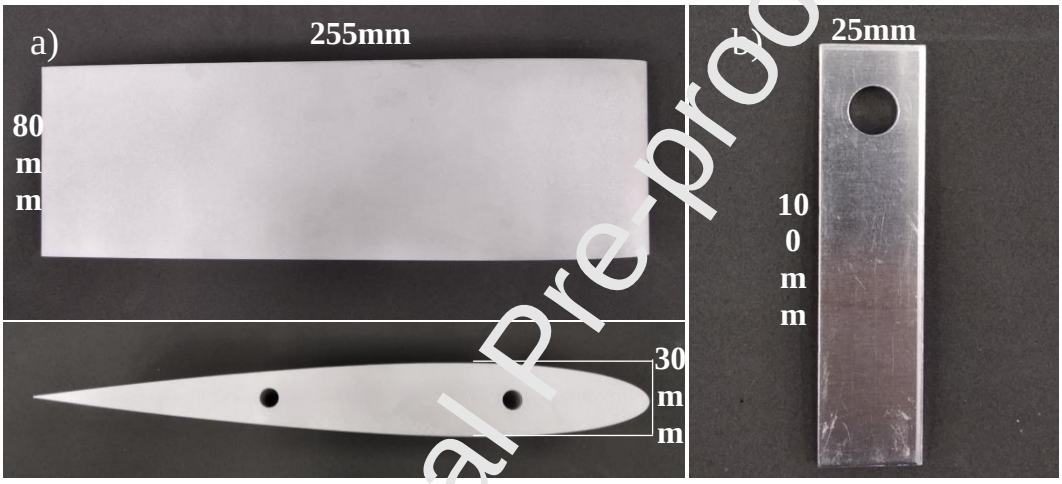

2

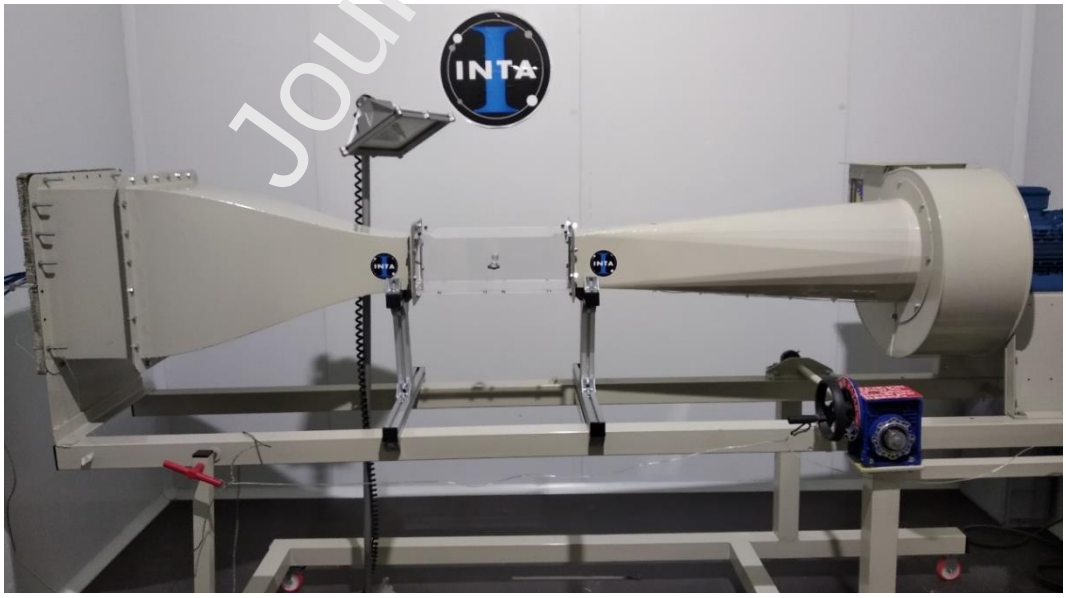

3

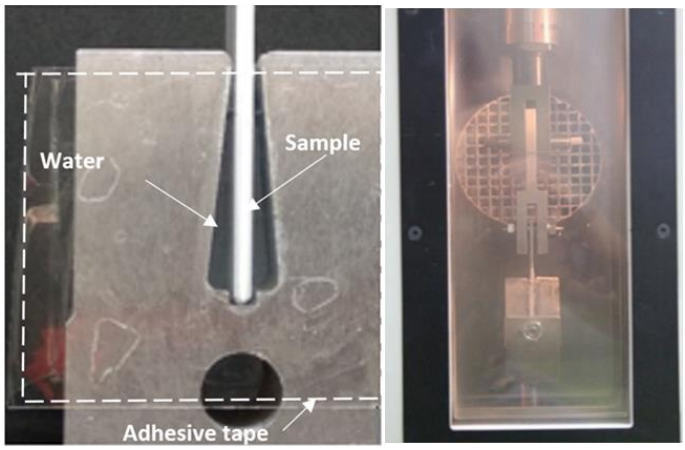

4

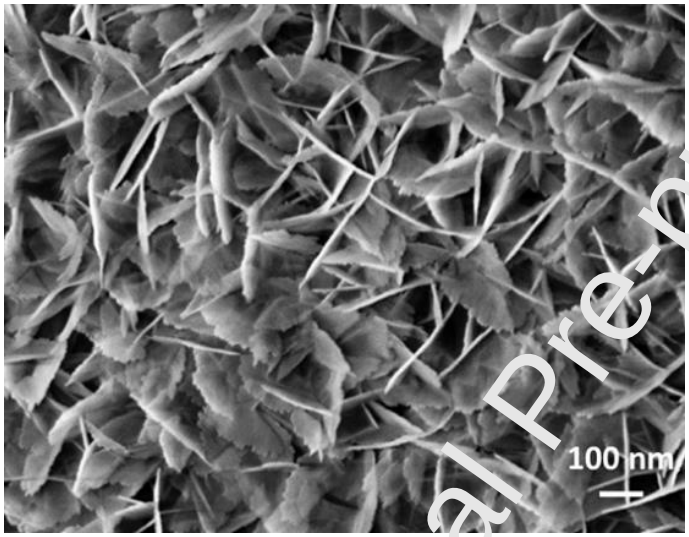

5

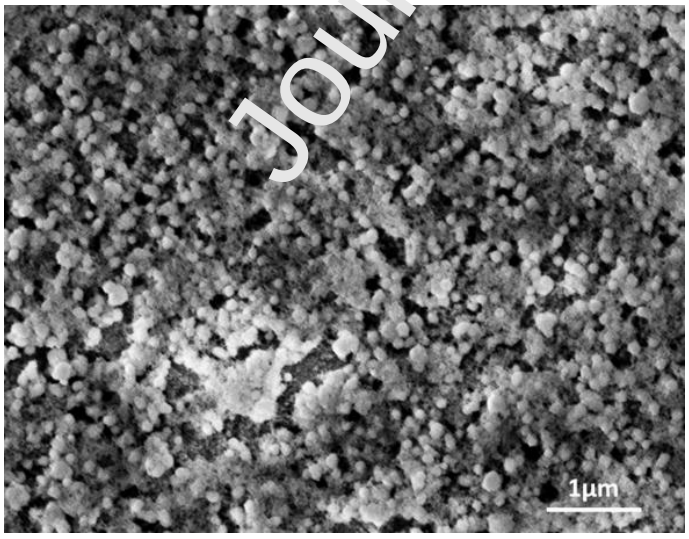

6

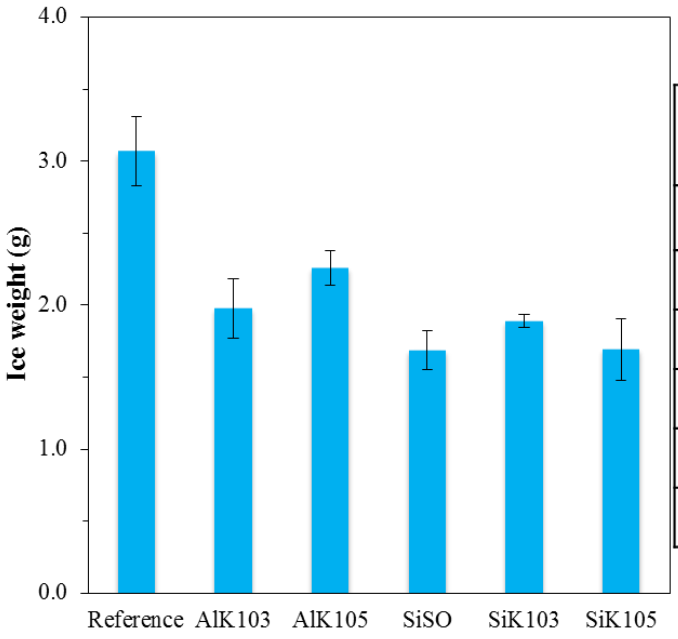

Sample	Ice weight (g)	Ice weight reduction (%)
Reference	3.07 ± 0.17	
AlK103	1.98 ± 0.21	35.5 ± 6.7
AlK105	2.26 ± 0.12	26.3 ± 4.0
SiSO	1.69 ± 0.14	45.0 ± 4.4
SiK103	1.89 ± 0.05	38.4 ± 1.5
SiK105	1.69 ± 0.22	44.8 ± 7.0

7

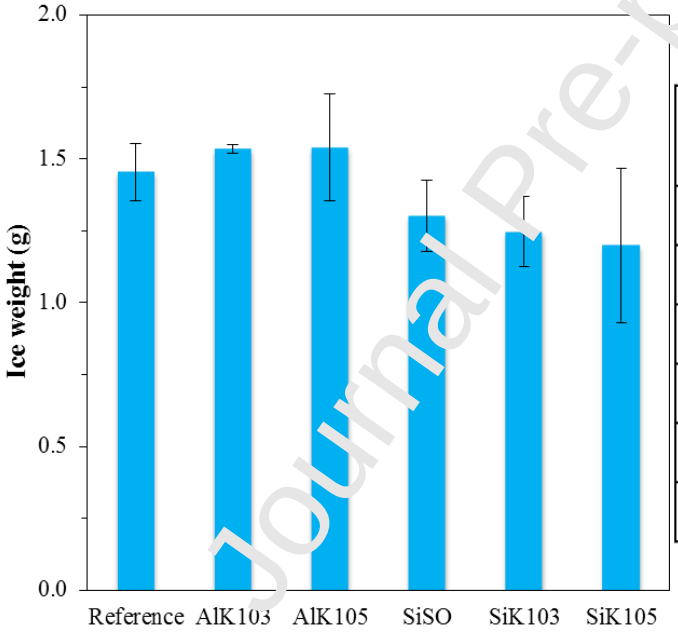

Sample	Ice weight (g)	Ice weight reduction (%)
Reference	1.45 ± 0.10	
AlK103	1.53 ± 0.02	-5.4 ± 1.1
AlK105	1.54 ± 0.19	-5.8 ± 12.9
SiSO	1.30 ± 0.12	10.4 ± 8.5
SiK103	1.25 ± 0.12	14.3 ± 8.4
SiK105	1.20 ± 0.27	17.5 ± 18.5

8

9

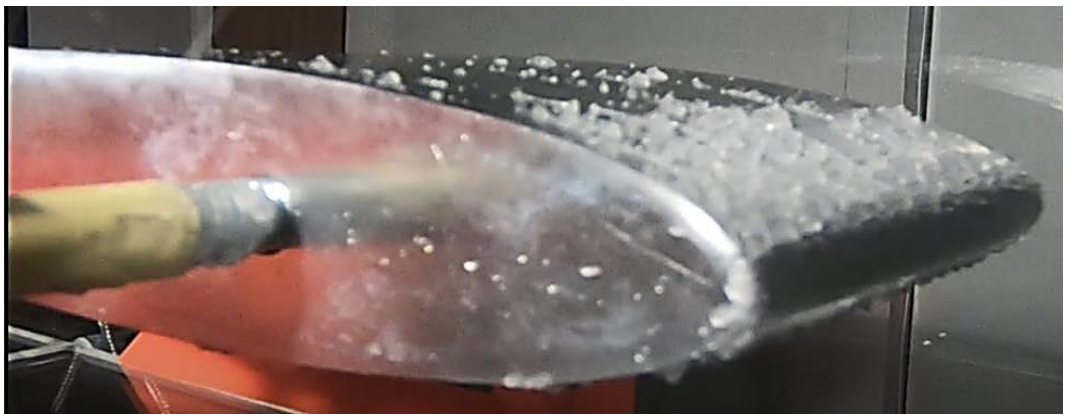

10

11

12

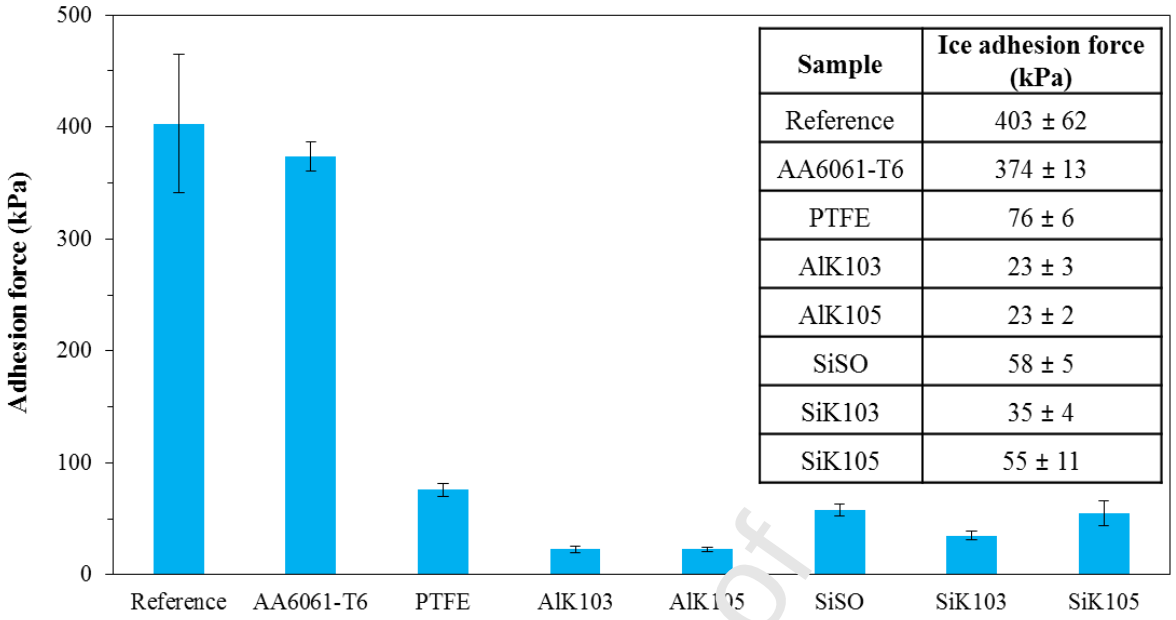

Sample	Ice adhesion force (kPa)
Reference	403 ± 62
AA6061-T6	374 ± 13
PTFE	76 ± 6
AlK103	23 ± 3
AlK105	23 ± 2
SiSO	58 ± 5
SiK103	35 ± 4
SiK105	55 ± 11

CRediT roles of authors

Federico Veronesi: Conceptualization, Formal analysis, Resources, Writing - Original Draft, Writing - Review & Editing, Visualization
Giulio Boveri: Conceptualization, Methodology, Formal analysis, Investigation, Resources, Writing - Original Draft, Writing - Review & Editing, Visualization, Project administration
Julio Mora: Methodology, Validation, Formal analysis, Investigation, Resources, Writing - Review & Editing, Visualization, Project administration
Alessandro Corozzi: Investigation, Writing - Review & Editing
Mariarosa Raimondo: Conceptualization, Resources, Writing - Review & Editing, Supervision, Project administration, Funding acquisition

Declaration of interests

☒The authors declare that they have no known competing financial interests or personal relationships that could have appeared to influence the work reported in this paper.

☐The authors declare the following financial interests/personal relationships which may be considered as potential competing interests:

Highlights

- Fabrication of anti-wetting, liquid-infused surfaces with different characteristics
- Coatings show reduced glaze ice accretion in icing wind tunnel tests
- Ice adhesion is reduced by an order of magnitude on coated surfaces